Journal of Advanced Ceramics
2012, 1(3): 204-220
DOI: 10.1007/s40145-012-0022-0 ISSN 2226-4108

Research Article

Synthesis of advanced ceramics by hydrothermal crystallization and modified related methods

José ORTIZ-LANDEROS[a], Carlos GÓMEZ-YÁÑEZ[a], Rigoberto LÓPEZ-JUÁREZ[b,*], Iván DÁVALOS-VELASCO[a], Heriberto PFEIFFER[c]

[a]*Departamento de Ingeniería Metalúrgica , Escuela Superior de Ingeniería Química e Industrias Extractivas, IPN, UPALM, Av. Instituto Politécnico Nacional s/n, CP 07738, México DF, México.*
[b]*Centro de Ciencias Aplicadas y Desarrollo Tecnológico, Universidad Nacional Autónoma de México, A.P. 70-186, Coyoacán, México D.F., México.*
[c]*Instituto de Investigaciones en Materiales, Universidad Nacional Autónoma de México, Circuito exterior s/n, Ciudad Universitaria, Del. Coyoacán, CP 04510, México DF, México.*

Received August 29, 2012; Accepted October 9, 2012

Abstract: The present article aims to give a brief overview about the advantages of the hydrothermal crystallization method for the synthesis of advanced ceramics. Emphasis is given, not only on the conventional hydrothermal crystallization, but also on some of its variants; such as ultrasound-assisted, electrochemical-assisted, microwave-assisted and surfactant-assisted hydrothermal methods which open up new opportunities for the synthesis of ceramic materials with novel properties demanded for advanced applications. In the current work the synthesis of barium titanate ($BaTiO_3$), lithium metasilicate (Li_2SiO_3) and sodium-potassium niobate (Na, K)NbO_3 powders are reported as cases of study.

Key words: hydrothermal synthesis; barium titanate; Li_2SiO_3; potassium-sodium niobate

1 Introduction

A general definition of hydrothermal process has been proposed by K. Byrappa and M. Yoshimura as follow: "the term hydrothermal refers to any heterogeneous chemical reaction in the presence of a solvent (whether aqueous or nonaqueous) above room temperature and at pressure greater than 1 atm in a closed system" [1]. In spite of this definition, which reaches a good consensus describing any hydrothermal process, it is important to keep in mind that depending on the field of study it is possible to find several other related terms. An example of this is the term *alcothermal* that makes reference to the type of solvent used [2].

The initial work related to hydrothermal synthesis of materials is attributed to R. W. Bunsen, who grew barium and strontium carbonate at temperatures above 200 ℃ and pressures above 100 bars in 1839. After that in 1845, E. Schafhautl [3] observed the formation of small quartz crystals upon transformation of precipitated silicic acid in a steam digester, the forerunner of the autoclave. Actually, the earliest

* Corresponding author.
E-mail: rigobertolj@yahoo.com.mx

studies on hydrothermal reactions were carried out by geologists in order to understand the petrogenesis of metamorphic rocks and minerals under hydrothermal conditions [2-5], and it wasn't until the 1940's that more intensive work about hydrothermal synthesis began with the preparation of single crystals of quartz and zeolites [1]. An interesting historical review about the first systematic studies carried out involving hydrothermal reactions was reported by R. Roy and O. F. Tutle [6].

Nowadays, the conventional hydrothermal method as well as its variants have emerged as a versatile synthesis option for the preparation of multifunctional ceramics materials including electronic ceramics, bioceramics, catalysts, catalyst supports, membranes and ceramics with optical properties, among others [1,2,7-18].

The main advantage of hydrothermal synthesis over the conventional ceramic process of solid state reaction is the lower temperatures of reaction. In fact, in addition to precursor phase preparation, pure and well crystallized materials can be synthesized directly by hydrothermal reactions, thus avoiding further thermal treatments (i.e., hydrothermal crystallization) [19-23]. This characteristic offers the possibility to obtain submicrometric and even nanometric or nanostructured materials [2,24].

In addition, hydrothermal crystallization also shows some advantages over other non-conventional processes of soft chemistry, such as sol-gel and coprecipitation. For instance, in hydrothermal crystallization the reaction times are shorter with a good control of the crystallization, crystal size, purity and even morphology of the products [25].

1.1 Conventional hydrothermal crystallization

In a typical hydrothermal synthesis, precursors are commonly prepared as solutions or suspensions, which are subsequently treated under autogenously pressures reached by using an autoclave vessel. Hydrothermal crystallization can be split into two stages, i.e., dissolution-supersaturation and subsequent crystallization [26]. In the first stage, dissolution of the precursor is promoted by both temperature and pressure, giving place to the formation of species in solution which are more prone to react and obtain the desirable product. This is assumed to be a stable phase under the selected hydrothermal conditions once the critical nucleation occurs.

For instance, the synthesis of a metal oxide under hydrothermal conditions can be visualized as follows [3]. At the beginning of the process as the temperature is increased, the hydrolysis of a metal salt precursor produces metal hydroxides. Then, when the system has reached a more elevated temperature the hydroxides are dehydrated, yielding the metal oxide. This is favored by the decrease of the dielectric constant of water and the increase of the oxygen solubility in water due to the critical conditions.

During the crystallization stage, particle growth is also present and takes place by re-dissolution and re-precipitation of the already formed phases. The growth of larger crystals is observed from those of smaller size, which is assumed to have a higher solubility. This phenomenon is known as Oswald ripening [27] and it happens during the second stage of the whole process. However, it is important to mention that nucleation and growth of amorphous phases or intermediate phases that are kinetically favored may takes place with further crystallization of the desirable phase only after longer periods of time. Based on this, it is clear that in a conventional hydrothermal synthesis, the composition of the precursor solution, temperature (including heating rate and reaction temperature), vessel pressure, and reaction time are the principal variables of any hydrothermal process.

In order to improve the performance of the conventional process, several techniques have been coupled with the hydrothermal crystallization method. In general, the resulting hybridized synthesis methods, such as ultrasound-assisted hydrothermal, electrochemical-assisted hydrothermal, microwave-assisted hydrothermal and surfactant-assisted hydrothermal techniques, can offer additional advantages over the conventional hydrothermal method. These include the reduction of reactions times and energy savings. This may also modify the characteristics of the products, such as purity, particle size, particle size distribution and morphology.

1.2 Ultrasound-assisted hydrothermal crystallization

This technique could be performed such as an ultrasound pretreatment of precursor solution and its further hydrothermal crystallization or the simultaneous use of ultrasound under hydrothermal conditions [28]. In both cases, the main benefits are the increase of the reaction kinetic and obtaining small

particle sizes. For example, Meskin *et al*. [29] successfully prepared the pure monoclinic phase of hafnium oxide (HfO_2) by ultrasound-assisted hydrothermal method at 250 ℃ for 0.5 h. It was observed that by using conventional methods, the crystallization process takes more than 3 h and the obtained product contains small quantities of a secondary amorphous phase. In the same manner, Rujiwatra *et al*. [30], prepared nanoparticles of the lead titanate ($PbTiO_3$) perovskite. In this case, an ultrasound pretreatment of the precursor solution promoted the crystallization of the phase at low temperature (130 ℃) and short hydrothermal reaction time (3.5 h). As in the single sonochemical reaction cases, the acustic cavitation phenomena and its related cavitational heating is believed to be the cause of the reaction rate improvement [31,32]. Other advantages attributed to the process are the possible formation of especial morphologies such as nanotubes [33], as well as the feasibility to prepared doped materials such as in the case of Fe-doped mesoporous TiO_2 [34].

1.3 Electrochemical-assisted hydrothermal crystallization

Electrochemical-assisted hydrothermal crystallization is a useful technique to fabricate crystalline ceramic thin films. The main advantages attributed to the technique are improved purity of the products, lower reaction temperature and higher film growth rates [4,35-43]. Moreover, film microstructures can be controlled by changing synthesis parameters such as the electrolyte temperature and composition, current loading time, and current density. Additionally, since the ceramic films, anodically grown, are affected by the dissolution-recrystallization process under hydrothermal conditions can show different microstructures specially from the point of view of the morphology and grain size of the films [35,36]. For instance, Wu and Yoshimura [36] observed the formation of multilayer microstructures in the case of $BaTiO_3$ films fabricated by the hydrothermal-electrochemical technique. This fact was explained by the competing reaction between the rate of the growth of anodic Ti-oxide films and the rate of precipitation from supersaturated $BaTiO_3$ particles.

Hill *et al.* [37] prepared several MnO_2 compounds with different crystalline phase (α, β and γ phases), as well as a number of different morphologies for the same phase (γ-MnO_2), such as needle-like and rod-like fibers. Different crystalline phase and morphology were obtained by controlling the synthesis parameters such as pH, temperature and applied current density.

The technique also offers the possibility to prepare more complex oxides, e.g., $LiNiO_2$ [38], solid solutions such as those reported by Masahiro Yoshimura ($Ca_{1-x}Sr_xTiO_3$) [39], doped materials such as Eu^{3+}:YVO_4 [40], and composite materias exposing good distribution of their components, such as hydroxyapatite/Ti [41] and hydroxyapatite/TiO_2 [42] composites.

1.4 Microwave-assisted hydrothermal crystallization

The first studies about microwave-assisted hydrothermal crystallization were conducted by Komarneni *et al*. [44] who synthesized different ceramic particles including TiO_2, ZrO_2, Fe_2O_3, $KNbO_3$ and $BaTiO_3$, and subsequently, several electroceramic powders such as $SrTiO_3$, $Sr_{0.5}Ba_{0.5}TiO_3$, $PbTiO_3$, $BaZrO_3$, $SrZrO_3$, $Pb(Zr_{0.52}Ti_{0.48})O_3$, and pyrochlore phases with formula $Pb(Mg_{1/3}Nb_{2/3})O_3$ and $Pb(Zn_{1/3}Nb_{2/3})O_3$ [45]. In these studies, authors observed several advantages over the conventional technique such as a significant reduction of reaction times and, in some cases, the formation of different crystalline phases than those obtained by the conventional hydrothermal route. They suggested that the success of the technique is due to the feasibility of microwave heating to dissolve the precursors during the hydrothermal reaction.

Actually, the use of microwave-assisted reactions in chemical synthesis is mainly based on the efficient heating by microwave irradiation [46]. In fact, in the case of microwave-assisted hydrothermal processes, microwave heating enhances the preparation of ultrafine and monodispersed powders. This is due to the fact that volumetric heating eliminates the thermal gradients, which favors a homogeneous nucleation and growth processes during the hydrothermal reaction. In addition, the microwave-assisted hydrothermal process enhances the product's purity and its affordability.

Some of the materials obtained via this method include $BaTiO_3$, wherein the use of microwave heating promotes the tetragonal phase of the powders [47,48] as well as the preparation of polycrystalline and homogeneous $BaTiO_3$ thin films grown on Ti-covered polymer substrates [49]. Microwave-assisted

hydrothermal reactions have been used for the synthesis of zeolite materials with special morphologies [50]: cerium carbonate hydroxide ($Ce(OH)CO_3$) showing hexagonal-shaped microplates [51], well-dispersed nanometric TiO_2 particles [52], nitrogen doped TiO_2 nanoparticles [53], Ni- and Zn-ferrite powders [54], nanosized bismuth tungsten oxide Bi_2WO_6 [55], $AgIn_5S_8$ nanoparticles with photocatalytic properties [56], well crystalline barium strontium titanate ($Ba_{0.8}Sr_{0.2}TiO_3$) [57], Yb^{3+} and Tm^{3+} co-doped β-$NaYF_4$ phase [58]. Other examples are the synthesis of binary mixed metal oxides having composition of $Ce_{0.75}Zr_{0.25}O_2$ [59], rod-like $LiMnO_2$ nanocrystals [60], high purity Hectorite clays materials [61] and mixed Co_3O_4/CoO nanorods [62].

Finally, another interesting feature of microwave heating is its selective heating characteristic. Since different materials show different abilities to absorb microwave energy and to convert it into heat (loss factor), this phenomenon could be useful to select a suitable reaction system. Therefore, a reaction medium with high microwave absorbing properties can be chosen looking forward to efficient and rapid heating. The use of ionic liquids as solvents for hydrothermal reactions is a good example of this. In the same sense, the loss factor phenomena is the reason why some ferrite materials can be synthesized at low temperatures only when microwave heating is used [63]. Cao *et al*. [64] prepared successfully $ZnFe_2O_4$ nanoparticles, iron hydroxyl phosphates ($NH_4Fe_2(PO_4)_2OH•2H_2O$) nanostructures [65] as well as α-FeOOH hollow spheres and α-Fe_2O_3 nanoparticles [66] via microwave- assisted hydrothermal ionic liquid synthesis. Other synthesized materials are Fe_3O_4 nanorods [67] and SnO_2 microspheres [68].

1.5 Surfactant-assisted hydrothermal crystallization.

The use of surfactants coupled with different routes of chemical synthesis has been used to control the crystallization of single particles, as well as to promote the ordering of these into more complex microstructures [69-74]. The surfactant-assisted hydrothermal method is a clear example of a bottom-up method for the synthesis of nanostructured ceramics [3,25], wherein different products exposing unique morphologies could be obtained as a result of surfactant acting as soft templates or growth-directing agent [71,75-87]. For instance, Zhao *et al*. [75] prepared crystalline calcium carbonate particles ($CaCO_3$) through the surfactant-assisted hydrothermal method. The obtained materials show several morphologies by using different solvents as well as different surfactants. The various morphologies include flower-like, belt-like, network-like, coralloid, and hexagonal morphologies, all of which exhibit different textural properties. The formation of the ordered superstructures takes place by a preferential aggregation mechanism due to the surfactants interaction with the primary formed nanoparticles.

Xu *et al*. [76] successfully synthesized γ-Bismuth molybdate (Bi_2MoO_6) powders. It was observed that when the conventional hydrothermal route was used, ultrafine particles with particle sizes in the range of 100 to 200 nm were obtained. On the other hand, when poly vinyl pyrrolidone (PVP) was used as surfactant, powders exposing nanoplate morphology were formed, resulting in unusual optical properties.

Meng *et al*. [77] prepared crystalline $BiVO_4$ with polyhedral, rod-like, tubular, leaf- like and spherical architectures via surfactant -assisted hydrothermal method by using the triblock copolymer P123. When the different samples were tested for the photodegradation of methylene blue, a remarkable influence of the morphology on the catalytic performance was observed.

García-Benjume *et al*. [78] prepared TiO_2-Al_2O_3 mixed oxides via hydrothermal synthesis using Tween-20 as a microstructure directing agent. The synthesized powders presented an unusual hierarchical macro-mesoporous microstructures. The authors propose a formation mechanism where supramolecular arrays of surfactant (both vesicles and micelles) act as soft templates promoting the porous superstructures.

Another examples of hydrothermal synthesis wherein the use of several surfactants plays a key role in the formation mechanism of complex microestrustures and novel properties are as follows: synthesis of Bi_2Te_3 [79], silica microspheres with MCM 41 porous microstructure[71], $BiVO_4$ photocatalysts [80], alumina nanotubes [81], hydroxyapatite nanoparticles [82], α-Fe_2O_3 nanoparticles [83], $CoFe_2O_4$ nanorods [84], YVO_4:Eu^{3+} powders [85], ZnO nanowires and nanopowders [86,87] and lamellar ultrafine magnesium hydroxide [88].

The present work aims to shows the advantages of the hydrothermal crystallization method for the synthesis of advanced ceramics. Three cases studies are discussed, i.e., the preparation of ultrafine barium

titanate ($BaTiO_3$) powders via the conventional hydrothermal method, the synthesis of lithium metasilicate (Li_2SiO_3) via surfactant-assisted hydrothermal crystallization, and finally the preparation of sodium-potassium niobate (Na, K)NbO_3 powders via microwave-assisted hydrothermal crystallization.

2 Experimental

2.1 Low temperature synthesis of $BaTiO_3$ ultrafine powders via conventional-hydrothermal method

In spite of the fact that ceramic materials have been obtained by the conventional hydrothermal (CH) route since mid-19th century, it was not until 1955 that the first barium titanate synthesis was recorded, which was based on hydrothermal crystallization from a titanium ester in an aqueous solution of barium soluble salt [4,89]. Since then a variety of ferroelectric and other electroceramics have been synthesized under different hydrothermal environments [89]. For the preparation of barium titanate (BT), a great variety of precursors has been used such as titanium dimetoxy-dineodecanoate with $Ba(OH)_2$ [90], titanium peroxo-hydroxide ($TiO_2(OH)_2$ with $Ba(OH)_2$•$8H_2O$ [91]), TiO_2 anatase with $Ba(OH)_2$•$8H_2O$ [92-94], $TiCl_4$ with $BaCl_2$•$2H_2O$ [95], titanium loaded polymer support with $Ba(OH)_2$ [95] and mineralizers such as KOH [4,94], NaOH [96], NH_4OH [95] while in some cases, $Ba(OH)_2$ hydrated or anhydrous was used as basic pH regulation source [90-91,93].

2.1.1 Synthesis and characterization of $BaTiO_3$ powders

Fine $BaTiO_3$ powders were synthesized by using anhydrous barium hydroxide $Ba(OH)_2$ and titanium oxide TiO_2 as precursors. $Ba(OH)_2$ was used not only as a source of Ba but also to adjust pH and then to promote solubility [90-91,93]. Precursors were charged into a teflon-lined autoclave. The Ba/Ti molar ratio in the mixed solution was fixed at 1 using a concentration ratio of $mBa(OH)_2$=$mTiO_2$=0.5. The pH obtained in the aqueous solution precursor was 12. Subsequently, the reactor was heated to temperatures between 90 ℃ and 180°C for different reaction times of 48 and 72 h. The obtained powders were washed with distilled water to remove soluble components and then dried at 100 ℃ for 24 h.

Later, in a second step, the obtained powders were sintered via the spark plasma sintering (SPS) process. Powder was poured into a graphite die and sintered following a heating rate of 200 ℃/min under uniaxial pressure of 40 MPa. High pulse sequence current of 3000 A and 3.5 V were utilized. The sintering temperature was 1100 ℃ at a holding time of 3 min. The crystalline structure and phase of the as-prepared and heat-treated powders were identified by X-ray powder diffractometry (XRD, Cu-K_a). Size and morphologies of powders were examined by high resolution scanning-transmission electron microscopy HRSTEM techniques.

2.1.2 Results and discussion

X-ray diffraction analysis indicates that crystalline BT phase can be obtained successfully at temperatures from 90 ℃ to 180 ℃ and times from 48 h to 72 h. Figure 1 shows XRD patterns and estimated crystallite sizes, of the series of samples synthesized by hydrothermal reaction at 72 h; only a small quantity of $BaCO_3$ was detected as secondary phase (Fig. 1a). Figure 1b shows crystallite sizes of different samples which were estimated based on the broadening of XRD pattern profiles by using the Scherrer's equation. In general, crystallite size augments with increasing the reaction temperature from 90 ℃ to 180 ℃. As expected, higher temperature and longer times results in bigger growth of crystallite.

The HRSTEM technique (Fig. 2) has shown in detail the particle size and morphology of powders obtained at different hydrothermal reaction times. In fact HRSTEM has shown that BT powders are constituted particles in the nanometric scale. It is revealed that reaction time has an effect on both particle size and morphology. Samples obtained at 48 h show a polygonal morphology with a main particle size of 75 nm. On the other hand, samples obtained at 72 h are spherical with a particle size of about 130 nm. HRSTEM analysis revealed that BT particles are made of crystallites smaller than 50 nm, or in other words single particles are constituted of small coherent crystalline domains (Fig. 2b inset) the aforesaid can explain the crystallite size values estimated by XRD technique. For all the cases, samples prepared via CH synthesis have a significantly smaller particle size with respect to samples prepared via solid state reaction, which commonly shows a particle size in the range of microns.

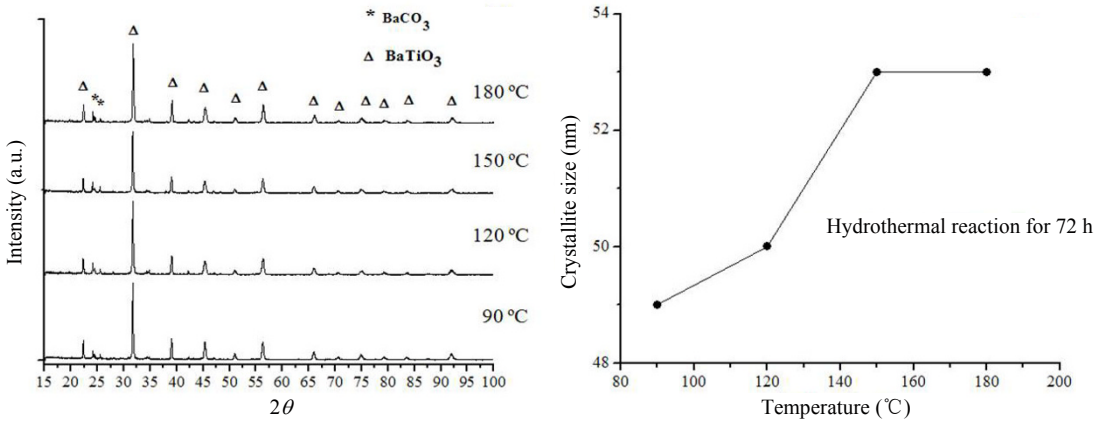

(a) (b)

Fig. 1 (a) XRD patterns of BT produced by CH at 72 h and different temperatures, and (b) crystallite size comparison of BT produced via CH as a function of the reaction temperature.

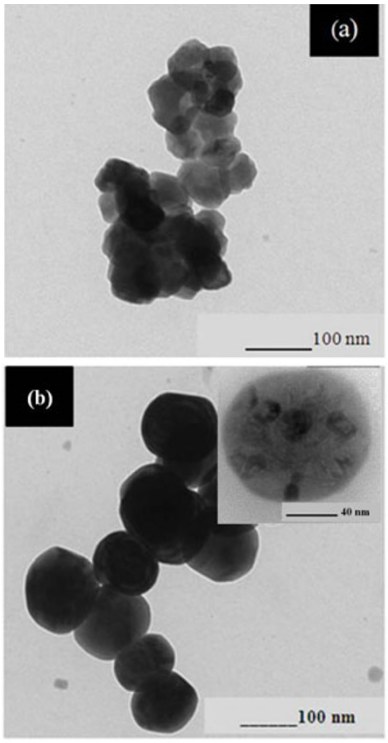

Fig. 2 HRSTEM micrograph of BT particles produced by CH method: (a) 48 h and (b) 72 h of reaction at 180 ℃.

Finally, dense ceramic bodies were successfully produced by using the synthesized powders. With the use of Spark Plasma Sintering technique, densities of 95.88% of theoretical values were obtained for the ceramic bodies fabricated. These characteristics are desirables from the point of view that high density reduces the effect of pores on weakening dielectric constant. In addition, the transforming fraction increases with the decrease of grain size.

Summarizing, BT is able to be synthesized at low temperature using the hydrothermal method. The obtained powders are nanocrystalline and present a fine particle size. These characteristics offer the advantage of obtaining homogeneous and fine grain size microstructures throughout the sintering process.

2.2 Synthesis of Li_2SiO_3 hollow microspheres via surfactant-assisted hydrothermal crystallization

Lithium metasilicate has been the topic of several studies because of their potential application as tritium breeder material into the fusion reactors [97,98] as an ionic conductor [99,100] and as a candidate for luminescent materials [101,102]. In general, Li_2SiO_3 has been synthesized by the conventional solid-state reaction method, and only some chemical routes have been studied such as the sol-gel, microemulsion and combustion methods [103-105]. Similar to the case of other alkaline ceramics, it is complicated to prepare lithium ceramics with small particle sizes because of its tendency to sinter or to lose lithium through a sublimation process at high temperatures. In this sense, chemical synthesis routes provide the possibility to obtain unique microstructural and morphological characteristics and, therefore, new applications for these kind of materials. Here the preparation of Li_2SiO_3 by both surfactant-assisted hydrothermal approach (SAH) and solid-state reaction (SSR) is reported, establishing the effect of the synthesis route on the microstructural and textural characteristics of the resultant powders.

2.2.1 Synthesis and characterization of Li_2SiO_3 powders

For the synthesis of SAH sample, lithium hydroxide ($LiOH•H_2O$) and tetraethyl orthosilicate (TEOS, $Si-(OC_2H_5)_4$) were used as starting materials. The used surfactant was Octylphenol ethylene oxide condensate (TRITON X-114). In the first step, certain quantity of the select non-ionic surfactant and LiOH reagents were dissolved in an ethylic alcohol aqueous solution. Later, stoichiometric amount of TEOS was added drop wise to the solution under mechanical stirring, followed by continuous stirring in an ultrasonic bath for 15 min. The obtained homogeneous gel was transferred into a Teflon-lined stainless steel autoclave vessel. The hydrothermal reaction was performed under autogenously produced pressure at a temperature of 100 ℃ for 20 h.

For the preparation of SSR samples the starting materials silicic acid (H_2SiO_3) and lithium carbonate (Li_2CO_3) were mixed in a mortar and calcined at 1000 ℃ for 7.5 h. After which time the powders were ground milled again before repeating the thermal treatment. Samples were characterized by XRD, SEM, TEM, and N_2 adsorption techniques.

2.2.2 Results and discussion

In order to reduce the number of experiments for obtaining the desirable pure phase of Li_2SiO_3, Eh-pH diagrams were constructed. Eh-pH diagrams show the stability region for the different stable ionic and nonionic species in aqueous solutions. The information is displayed as a plot of pH versus electrochemical potential, and it can be used as a simple resort to estimate phase equilibrium during the hydrothermal processes [23,106-107].

In this same sense, another well documented and powerful resource to determine the optimum conditions in systematic synthesis studies related to hydrothermal processes are both phase stability and yield diagrams. However, their construction involves more complex thermodynamic calculations. Their construction and the thermodynamic fundamentals have been also well documented [108-110].

In the current work, the specific hydrothermal reaction conditions were chosen based on Eh-pH equilibrium diagram for the Li-Si-H_2O system only as a reference (Fig. 3). The Eh-pH diagram was drawn with the help of the FACT-Sage (Thermochemical Software and Databases) software [111], considering a total concentration of 0.8 molal and temperature of 100 ℃.

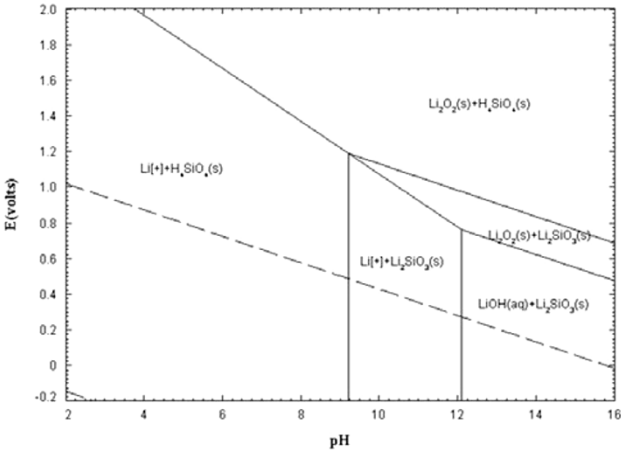

Fig. 3 Eh-pH diagram of the Li-Si-H_2O system showing predominance domains of species. Diagrams were obtained considering a metal's ratio of 0.2<Si/(Li+Si)<0.333, and temperature of 100 ℃.

The Eh-pH diagram reveals that the Li_2SiO_3 phase is stable at pH values up to ~9.2.

Figure 4 shows the XRD patterns of the different samples. The results show that both SSR and SAH samples correspond to Li_2SiO_3 phase (JCPDS card No. 29-0828). However, the SSR sample has a small impurity of lithium orthosilicate phase (Li_4SiO_4). In addition, the XRD pattern profiles show some differences mainly on the line broadening. This is attributed to certain differences on crystallite size as a result of the synthesis method, surfactant addition and synthesis temperature. In fact, based on the analysis of XRD patterns profiles, crystallite size were estimated

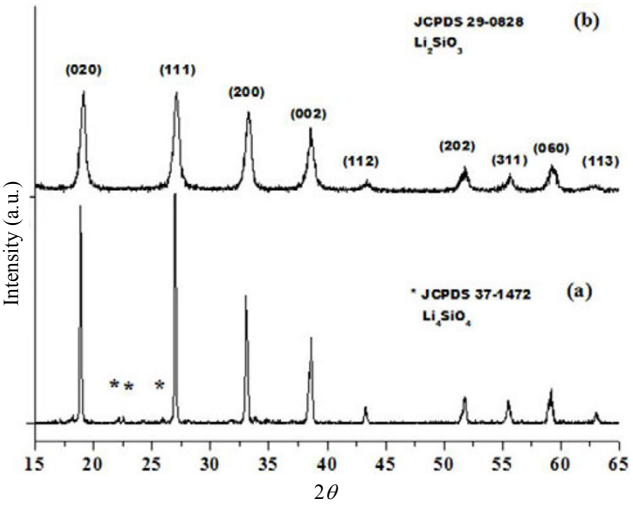

Fig. 4 XRD patterns of as prepared lithium silicate powders; the different samples are: (a) SSR, and (b) SAH.

as 14 nm and >50 nm for SAH and SSR samples, respectively.

SEM photomicrographs show a noticeable change in morphology due to different synthesis methods (Fig. 5). SSR powders present morphology of dense aggregates with particle size varying from 3 to as higher as 25 μm (Fig. 5a). On the other hand, SAH powders show well-defined spherical aggregates with particle size smaller than 3.5 μm (Fig. 5b). Another important feature is the fact that these powders present a hollow microstructure. Similar to other reported systems [27], the possible formation mechanism of the hollow Li_2SiO_3 microspheres is attributed that takes place via Oswald ripening mediated process.

Figure 6 shows the TEM image corresponding to the SAH synthesized sample. The contrast observed in the bright-field image shows the hollow microstructure (Fig. 6a). Spherical aggregates present diameters between 2 μm and 3 μm. The TEM electron diffraction pattern shows diffused rings, indicating that synthesized powders are polycrystalline (Fig. 6b). The SAED rings were indexed as the orthorhombic structure of Li_2SiO_3 according with the XRD JCPDS card No. 29-0828. In addition, TEM images revealed the formation of smaller and also hollow spheres about 400 nm. In general, these observations suggest the presence of different mechanism of formation of the aggregates. Among them, the formation of the smallest

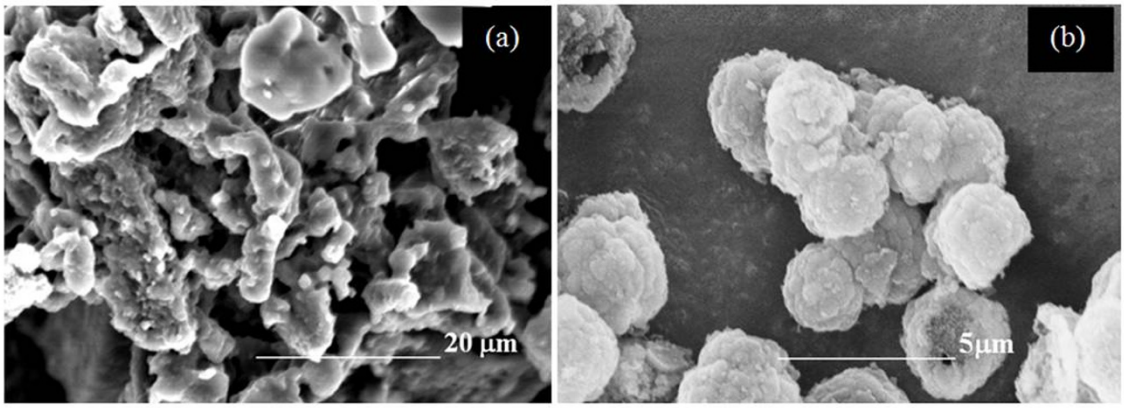

Fig. 5 (a) SEM images of samples prepared by solid state reaction and (b) surfactant-assisted hydrothermal methods.

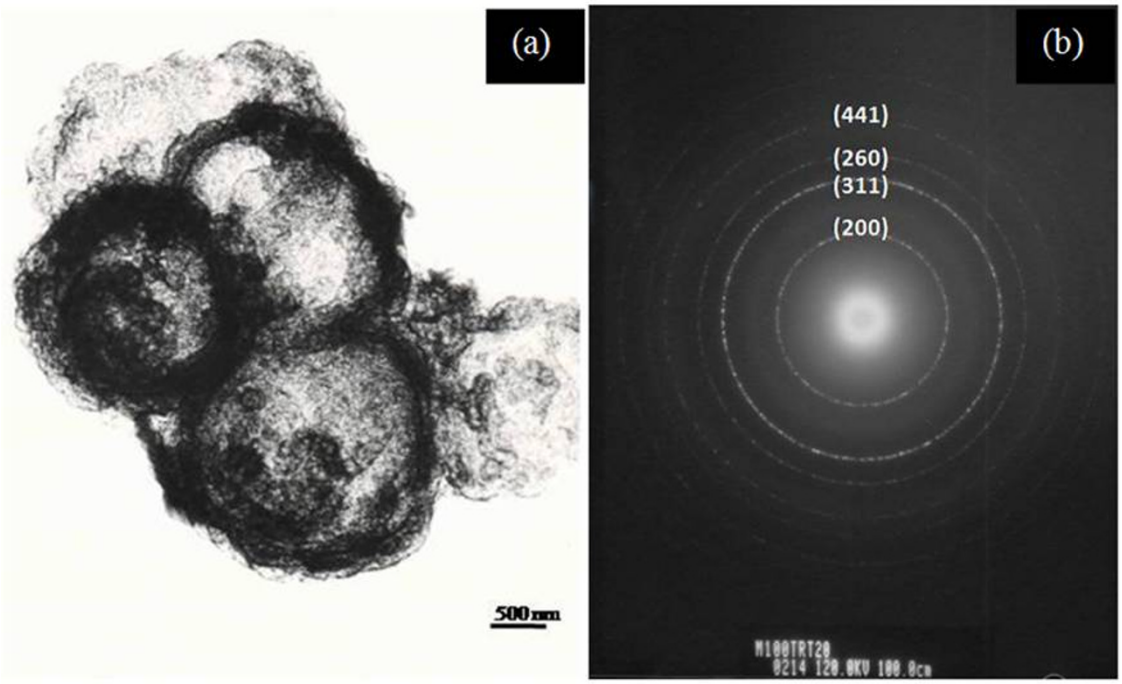

Fig. 6 (a) Bright field TEM image of sample SAH and (b) indexed SAEDP of Li_2SiO_3.

spherical aggregates is the result of the surfactant effect which plays the role of template. More details about the hydrothermal synthesis of Li_2SiO_3 in presence of different surfactants were previously reported [112].

Figure 7 shows adsorption-desorption isotherms corresponding to the different samples. According to the IUPAC classification [113-114], while the SSR sample shows a type III isotherm, the SAH sample presents a type II isotherm which can be attributed to a monolayer-multilayer adsorption on an open external surface of macroporous adsorbents. This sample shows a hysteresis loop type H3, which doesn't exhibit a limiting adsorption at high P/Po values. This fact is usually interpreted as a result of the presence of slit-like pores. In the current work this fact was attributed to the presence of interparticle voids. In addition, it is noticeable that in the case of the SAH sample, volume adsorbed increases considerably compared to the SSR sample (Fig. 7, see scale), which corroborates the formation of smaller and more porous particles. Additionally, specific surface values were calculated by BET model [115]. Samples exposed surfaces area values of 69.5 m^2g^{-1} and 0.47 m^2g^{-1} for SAH and SSR, respectively.

The microstructure and textural properties obtained through the surfactant-assisted hydrothermal synthesis route, suggests advantages with respect to the solid state reaction method. These pure and nano-crystalline Li_2SiO_3 may be suitable to be used for certain applications such as CO_2 absorption [103-105].

2.3 One step synthesis of $K_{0.5}Na_{0.5}NbO_3$ solid solutions via hydrothermal microwave-assisted method

Today, synthesis of lead-free piezoceramics is of strong interest when looking at a more environmentally friendly option for the fabrication of optical and acoustic devices such as optical wave-guiding and frequency doubling [116-120]. The different studies have been focused on the preparation of sodium-bismuth titanates and potasium-sodium-niobates (KNN) [117,121-124]. These studies included both pure and doped compounds. In fact, among them, KNN are the most promising because of their good piezoelectric properties as well as their high Curie's temperature values [125]. With respect to the synthesis, a common problem faced by using the conventional solid state reaction route is that potassium and sodium are lost by sublimation during the calcinations and sintering stages at elevated temperatures. This affects the stoichiometry of the final products promoting the presence of secondary phases [126]. Other synthesis methods have been studied as an alternative proposal, such as sol-gel [127,128], Pechini [129] and conventional hydrothermal [130,131]. Among them, the sol-gel and Pechini approaches present the disadvantages of involving expensive precursors which in some cases may also be difficult to handle, as in the case of alkoxides.

The conventional hydrothermal method has been used to prepare sodium niobate, potassium niobate and potassium tantalite [132-134]. However, this method

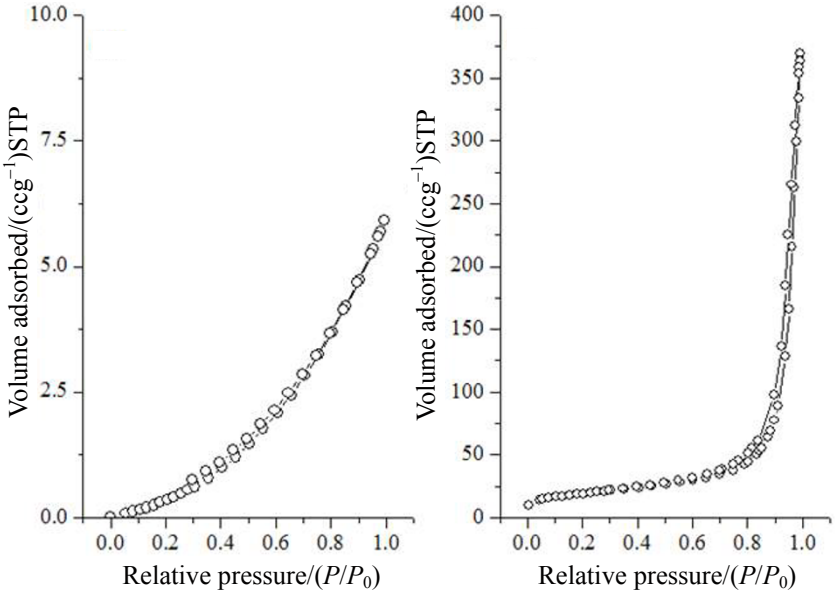

Fig. 7 N_2 physisorption isotherms of the prepared samples: (a) SSR, and (b) SAH.

also presents certain difficulties to obtain pure phases and compositional homogeneous products in one step, making it necessary to perform further thermal treatments [135].

In the present work, the synthesis of KNN by conventional hydrothermal (CH) and microwave-assisted hydrothermal (MAH) methods is reported.

2.3.1 Synthesis and characterization of $K_{0.5}Na_{0.5}NbO_3$ solid solutions

Potassium hydroxide (KOH ⩾ 90%), Sodium hydroxide (NaOH 99%) and niobium pentoxide (Nb_2O_5 99.99%) were used as starting materials. In the first step, an aqueous solution of (KOH+NaOH) was prepared. Based on previous studies [130,131], the molar ratio of 7.5:2.5 (KOH:NaOH) was chosen. After that, 2 grams of Nb_2O_5 were added to the alkaline solution. The formed suspension was stirred for 2 hours before the hydrothermal reaction.

For the synthesis of CH sample, the mixed precursor suspension was put in a Teflon-lined stainless steel autoclave, which was heated at 240 ℃ for 24 h by using an electric furnace and following a heating rate of 10 ℃/min. After that, the autoclave reactor was cooled to ambient temperature and the obtained powders were filtered, washed several times with deionized water and finally dried at 120 ℃ for 2 h.

Regarding the synthesis of MAH sample, a Teflon reinforced autoclave was used. The autoclave reactor was heated at 210 ℃ in a microwave oven CEM model MARS for 30 min, followed by a heating rate of 14 ℃/min. The power source in the oven was fixed at 800 W. After hydrothermal reaction, the washing and drying steps were carried out.

Structural and microstructural characterization of the powders was performed by XRD and SEM techniques.

2.3.2 Results and discussion

X-ray patterns corresponding to different synthesized samples are shown in Fig. 8.

It is noticed that when the conventional method was used two phases were obtained. The first one was identified as $KNbO_3$ (JCPDS 71-2171), and the second one as $NaNbO_3$ (JCPDS 01-074-2025). However, it is remarkable that for both phases, the obtained XRD patterns present certain shifts of their reflexions; this fact was clearly evident in the higher 2-thetha values peaks (see Fig. 8). This suggests that in both cases a partial degree of substitution ($Na^{+1}\leftrightarrow K^{+1}$) was promoted, so it can be expressed as the obtaining of the $K_xNa_{1-x}NbO_3$ (x>0.5) and $Na_{1-y}NbO_3$ (y<0.5) which are potassium and sodium enriched phases, respectively. On the other hand, the diffraction pattern of MAH sample shows only the peaks corresponding to the orthorhombic pure $KNbO_3$ perovskite phase (JCPDS 71-2171). Of course, in this case the reflexions also shift to higher two theta values due to the incorporation of Na into the crystalline structure of $KNbO_3$, and then the one-step formation of the $K_{0.5}Na_{0.5}NbO_3$ solid solution phase (Fig. 8b). Actually, in a recent study Maeda *et al*. [135] prepared (K, Na)NbO_3 lead-free piezoelectric ceramics by using previously CH synthesized powders. However, in this case thermal treatment was required for the solid solution formation. Therefore, this work is reported for the first time the use of microwave-hydrothermal processing for the preparation of this kind of materials in one step.

After that, CH powders were thermally treated at temperatures of 600 ℃ and 800 ℃ in order to obtain the $K_{0.5}Na_{0.5}NbO_3$ phase. Figure 9 shows the XRD patterns of the different samples.

Figure 9 shows the evolution of the KNN phase by both sodium and potassium diffusion among the solid particles throughout the further thermal treatments. In fact, the reaction can be described as follow:

$$n\mathrm{K}_x\mathrm{Na}_{1-x}\mathrm{NbO}_3+(1-n)\mathrm{K}_y\mathrm{Na}_{1-y}\mathrm{NbO}_3 \longrightarrow \mathrm{K}_{0.5}\mathrm{Na}_{0.5}\mathrm{NbO}_3 \quad (1)$$

where $K_xNa_{1-x}NbO_3$ (x>0.5) and $Na_{1-y}NbO_3$ (y<0.5) are the potassium and sodium enriched phases, respectively.

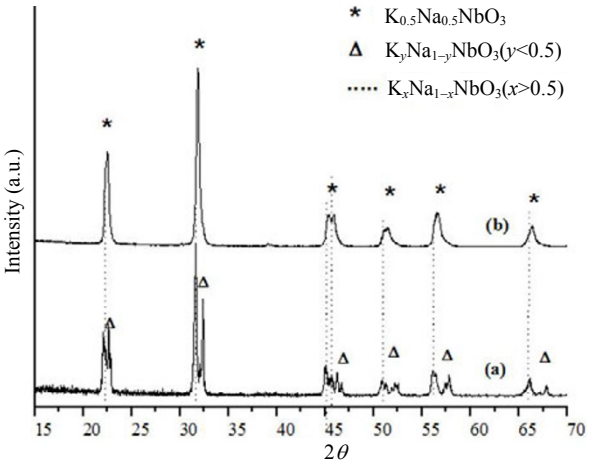

Fig. 8 KNN powders synthesized by: (a) conventional hydrothermal at 240 ℃ for 24 h, and (b) microwave-assisted hydrothermal at 210 ℃ for 30 min.

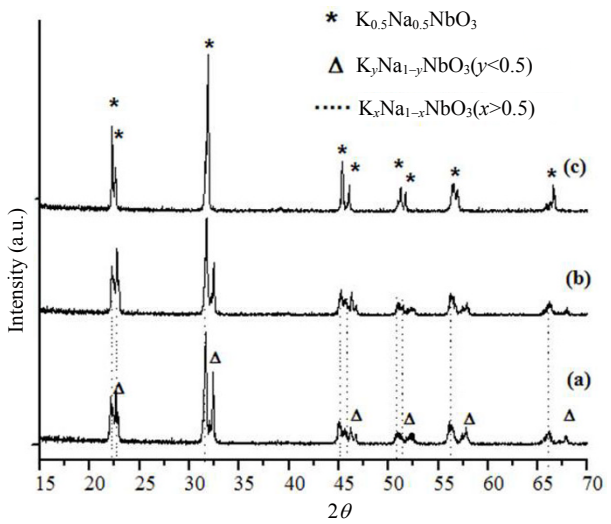

Fig. 9 XRD patters of CH samples: (a) as prepared powders, (b) calcined at 600 ℃ and (c) calcined at 800 ℃.

The complete formation of $K_{0.5}Na_{0.5}NbO_3$ from the CH powders was finally reached after calcinations at 800 ℃.

Finally, Figure 10 show the SEM images of KNN samples prepared by calcinations of CH powders at 800 ℃ and MAH sample.

Both samples are constituted by ultrafine powders with aggregates in the micrometric range. However, it is clear that smaller particles were obtained in MAH sample. In fact, this sample is constituted by submicrometric primary particles smaller than 500 nm (Fig. 10b). These results can be attributed to both the shorter time of hydrothermal reaction as well as the direct crystallization of KNN phase without thermal treatment.

Then summarizing, KNN powders with chemical composition of $K_{0.5}Na_{0.5}NbO_3$ are able to be successfully synthesized by the hydrothermal technique. The conventional method gives the possibility of obtaining ultrafine powders, and in fact, reduces the calcination temperature for the preparation of the solid solution. In addition, the microwave-assisted method offers not only the possibility to obtain high quality powders, but also to obtain well crystallized doped materials such as KNN powders with the advantages of shorter times and in one-step. In other words, further thermal treatment would not be necessary. This is attributed to the effect microwave heating has on the dissolution of the precursors and on the kinetic of crystallization of the final product during the different stages of the hydrothermal process.

3 Conclusions

The hydrothermal crystallization method for the synthesis of ceramics was reviewed. Conventional hydrothermal crystallization, surfactant-assisted and microwave–assisted hydrothermal methods were showed as promising methods for the preparation of ceramic powders with novel properties. The synthesis of $BaTiO_3$, Li_2SiO_3 and ((Na, K)NbO_3) powders were discussed as cases of study.

$BaTiO_3$ was successfully synthesized at low temperature. The effect of both temperature and reaction time on the crystallization and particle size were studied. The obtained powders show fine particle size in the nanometric range that can offer advantages for the fabrication of homogeneous and fine grain size microstructures through the sintering process.

Crystalline Li_2SiO_3 powders were synthesized using TRITON X-114 surfactant. Experimental conditions for obtaining the desirable pure phase of

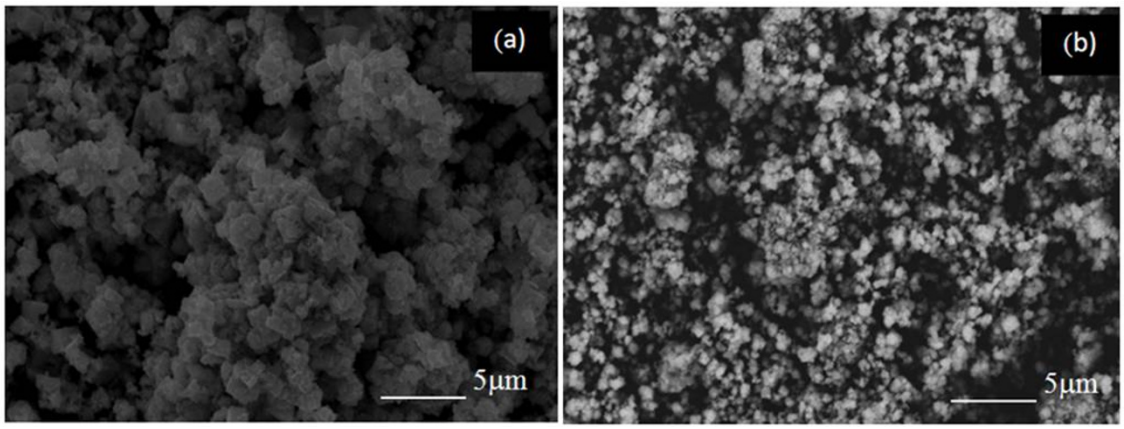

Fig. 10 SEM images of different samples: (a) CH after calcinations at 800 ℃ and (b) MAH powders.

Li_2SiO_3 were established base on the Eh-pH diagrams that constitute a simple resort to estimate phase equilibrium during the hydrothermal processes. The obtained powders show novel microstructures of hollow microspheres exposing high surfaces areas about 69.5 m^2g^{-1}.

Finally $K_{0.5}Na_{0.5}NbO_3$ solid solutions were synthesized by both the conventional and microwave-assisted hydrothermal methods. Conventional method produces ultrafine powders and reduces the temperature for the preparation of the solid solutions by further calcinations. Additionally, the used of microwaves-based heating offers the possibility to obtain well crystallized solid solutions with the advantages of short reaction times and in one-step, which avoids further thermal treatments.

Acknowledgment

The authors thank to SIP-IPN and SNI-CONACYT México for the financial support. Furthermore, the authors thank to Dr. J.J. Cruz Rivera and M.Sc. Tyler T. Norton for their technical help with TEM analyses and technical support on results discussion, respectively.

References

[1] Byrappa K, Yoshimura M. *Handbook of Hydrothermal Technology*. New York: William Andrew, 2001.

[2] Byrappa K, Adschiri T. *Progress in Crystal Growth and Characterization of Materials*. Amsterdam: Elsevier, 2007.

[3] Lalena JN, Cleary DA, Carpenter E, *et al*. *Inorganic Material Synthesis and Fabrication*. New Jersey: John Wiley & Sons Inc, 2008.

[4] Riman RE, Suchanek WL, Lencka MM. Hydrothermal crystallization of ceramics**.** *Ann Chim Sci Mat* 2002, **27**: 15-36.

[5] Bucher K, Frey M. *Petrogenesis of Metamorphic Rocks*. Berlin: Springer, 2002.

[6] Roy R, Tuttle OF. Investigations under hydrothermal conditions. *Phys Chem Earth* 1956, **1**: 138-180.

[7] Suchanek WL, Riman RE. Hydrothermal synthesis of advanced ceramic powders. *Advances in Science and Technology* 2006, **45**: 184-193.

[8] Tang XL, Xiao XF, Liu RF. Structural characterization of silicon-substituted hydroxyapatite synthesized by a hydrothermal method. *Mater Lett* 2005, **59**: 3841-3846.

[9] Yoshimura M, Sujaridworakun P, Koh F, *et al*. Hydrothermal conversion of calcite crystals to hydroxyapatite. *Mater Sci Eng C* 2004, **24**: 521-525.

[10] Zhang H, Zhu Q. Structure control in hydroxyapatite synthesis by hydrothermal reaction and organic modulators. *Particuology* 2005, **3**: 317-320.

[11] Hu X, Shen H, Cheng Y, *et al*. One-step modification of nano-hydroxyapatite coating on titanium surface by hydrothermal method. *Surf Coat Tech* 2010, **205**: 2000-2006.

[12] Wang H, Lin YS. Effects of synthesis conditions on MFI zeolite membrane quality and catalytic cracking deposition modification results. *Micropor Mesopor Mat* 2011, **142**: 481-488.

[13] Cundy CS, Cox PA. The hydrothermal synthesis of zeolites: Precursors, intermediates and reaction mechanism. *Micropor Mesopor Mat* 2005, **82**: 1-78.

[14] Whittingham MS, Guo JD, Chen R, *et al*. The hydrothermal synthesis of new oxide materials. *Solid State Ionics* 1995, **75**: 257-268.

[15] Panda SK, Chaudhuri S. Chelating ligand-mediated synthesis of hollow ZnS microspheres and its optical properties. *J Colloid Interf Sci* 2007, **313**: 338-344.

[16] López-Luke T, De la Rosa E, Sólis D, *et al*. Effect of the CTAB concentration on the upconversion emission of ZrO_2:Er^{3+} nanocrystals. *Opt Mater* 2006, **29**: 31-37.

[17] Yang JY, Su YC, Liu XY. Hydrothermal synthesis, characterization and optical properties of $La_2Sn_2O_7$:Eu^{3+} micro-octahedra. *Nonferrous Met Soc China* 2011, **21**: 535-543.

[18] Kim JR, Lee KY, Suh MJ, *et al*. Ceria–zirconia mixed oxide prepared by continuous hydrothermal synthesis in supercritical water as catalyst support. *Catal Today* 2011, **185**: 25-34.

[19] Ifrah S, Kaddouri A, Gelin P, *et al*. Conventional hydrothermal process versus microwave-assisted hydrothermal synthesis of $La_{1-x}Ag_xMnO_{3+\delta}$ (x = 0, 0.2) perovskites used in methane combustion. *CR Chimie* 2007, **10**: 1216-1226.

[20] Solís D, López-Luke T, De la Rosa E, *et al*. Surfactant effect on the up conversion emission and decay time of ZrO_2: Yb-Er nanocrystals. *J Lumin* 2009, **129**: 449-455.

[21] Zhang DR, Liu HL, Jin RH, *et al*. Synthesis and characterization of nanocrystalline $LiTiO_2$ using a one-step hydrothermal method. *J Ind Eng Chem* 2007, **13**: 92-96.

[22] Wang SM, Wang QS, Wan QL. Template-directed synthesis of MS (M=Cd, Zn) hollow microsphere via hydrothermal method. *J Cryst Growth* 2008, **310**: 2439-2443.

[23] Piticescu R, Monty C, Millers D. Hydrothermal synthesis of nanostructured zirconia materials: Present state and future prospects. *Sensor Actuat B* 2005, **109**: 102-106.

[24] Kaya C, He JY, Gu X, *et al*. Nanostructured ceramic powders by hydrothermal synthesis and their applications. *Micropor Mesopor Mat* 2002, **54**: 37-49.

[25] Yan C, Zou L, Xue D, *et al*. Chemical tuning polymorphology of functional materials by hydrothermal and solvothermal reactions. *J Mater Sci* 2008, **43**: 2263-2269.

[26] Schäf O, Ghobarkar H, Knauth P. *Nanostructured Materials: Selected Synthesis Methods, Properties and Applications*. Norwell: Kluwer Academic, 2002.

[27] Zeng HC. Ostwald ripening: A synthetic approach for hollow nanomaterials. *Current Nanoscience* 2007, **3**: 177-181.

[28] Meskin PE, Ivanov VK, Barantchikov AE, *et al*. Ultrasonically assisted hydrothermal synthesis of nanocrystalline ZrO_2, TiO_2, $NiFe_2O_4$ and $Ni_{0.5}Zn_{0.5}Fe_2O_4$ powders. *Ultrasonics Sonochem* 2006, **13**: 47-53.

[29] Meskin PE, Sharikov FY, Ivanov VK, *et al*. Rapid formation of nanocrystalline HfO_2 powders from amorphous hafnium hydroxide under ultrasonically assisted hydrothermal treatment. *Mater Chem Phys* 2007, **104**: 439-443.

[30] Rujiwatra A, Wongtaewan C, Pinyo W, *et al*. Sonocatalyzed hydrothermal preparation of lead titanate nanopowders. *Mater Lett* 2007, **61**: 4522-4524.

[31] Gedanken A. Using sonochemistry for the fabrication of nanomaterials. *Ultrason Sonochem* 2004, **11**: 47-55.

[32] Mason JT. Use of ultrasound in chemical synthesis. *Ultrasonics* 1986, **24**: 245-253.

[33] Manafi S, Nadali H, Irani HR. Low temperature synthesis of multi-walled carbon nanotubes via a sonochemical/hydrothermal method. *Mater Lett* 2008, **62**: 4175-4176.

[34] Li H, Liu G, Chen S, *et al*. Novel Fe doped mesoporous TiO_2 microspheres: Ultrasonic-hydrothermal synthesis, characterization, and photocatalytic properties. *Physica E* 2010, **42**: 1844-1849.

[35] Suchanek W, Watanabe T, Yoshimura M. Preparation of $BaTiO_3$ thin films by the hydrothermal-electrochemical method in the flowing solution. *Solid State Ionics* 1998, **109**: 65-72.

[36] Wu Z, Yoshimura M. Investigations on procedures of the fabrication of barium titanate ceramic films under hydrothermal-electrochemical conditions. *Solid State Ionics* 1999, **122**: 161-172.

[37] Hill LI, Verbaere A, Guyomard D. MnO_2 (α-, β-, γ-) compounds prepared by hydrothermal-electrochemical synthesis: characterization, morphology, and lithium insertion behavior. *J Power Sources* 2003, **119**: 226-231.

[38] Yoshimura M, Han KS, Tsurimoto S. Direct fabrication of thin-film $LiNiO_2$ electrodes in LiOH solution by electrochemical-hydrothermal method. *Solid State Ionics* 1998, **106**: 39-44.

[39] Yoshimura M, Asai O, Cho WS, *et al*. Low-temperature synthesis of crystallized $Ca_{1-x}Sr_xTiO_3$ solid-solution films on titanium substrates by a modified hydrothermal-electrochemical technique. *J Alloy Compd* 1998, **265**: 132-136.

[40] Watanabe T, Cho WS, Suchanek WL, *et al*. Direct fabrication of crystalline vanadates films by hydrothermal-electrochemical method. *Solid State Sciences* 2001, **3**: 183-188.

[41] Xiao XF, Liu RF, Zheng YZ. Hydoxyapatite/ titanium composite coating prepared by hydrothermal-electrochemical technique. *Mater Lett* 2005, **59**: 1660-1664.

[42] Xiao XF, Liu RF, Zheng YZ. Characterization of hydroxyapatite/titania composite coatings codeposited by a hydrothermal-electrochemical method on titanium. S*urf Coat Tech* 2006, **200**: 4406-4413.

[43] Agarwal S, Sharma GL. Humidity sensing properties of (Ba, Sr)TiO_3 thin films grown by hydrothermal-electrochemical method. *Sensor Actuat B* 2002, **85**: 205-211.

[44] Komarneni S, Roy R, Li QH. Microwave-hydrothermal synthesis of ceramic powders. *Mat Res Bul*l 1992, **27**: 1393-1405.

[45] Komarneni S, Li Q, Stefansson KM, *et al*. Microwave-hydrothermal processing for synthesis of electroceramic powders. *J Mater Res* 1993, **8**: 3176-3183.

[46] Bilecka I, Niederberger M. Microwave chemistry for inorganic nanomaterials synthesis. *Nanoscale* 2010, **2**: 1358-1374.

[47] Sun W, Li C, Li J, *et al*. Microwave-hydrothermal synthesis of tetragonal $BaTiO_3$ under various

conditions. *Mater Chem Phys* 2006, **97**: 481-487.

[48] Sun W, Li J. Microwave-hydrothermal synthesis of tetragonal barium titanate. *Mater Lett* 2006, **60**: 1599-1602.

[49] Tan CK, Goh GK, Lau GK. Growth and dielectric properties of $BaTiO_3$ thin films prepared by the microwave-hydrothermal method. *Thin Solid Films* 2008, **516**: 5545-5550.

[50] Hu Y, Liu C, Zhang Y, *et al*. Microwave-assisted hydrothermal synthesis of nanozeolites with controllable size. *Micropor Mesopor Mat* 2009, **119**: 306-314.

[51] Riccardi CS, Lima RC, Dos Santos ML, *et al*. Preparation of CeO_2 by a simple microwave-hydrothermal method. *Solid State Ionics* 2009, **180**: 288-291.

[52] Chen Z, Li W, Zeng W, *et al*. Microwave hydrothermal synthesis of nanocrystalline rutile. *Mater Lett* 2008, **62**: 4343-4344.

[53] Zhang P, Liu B, Yin S, *et al*. Rapid synthesis of nitrogen doped titania with mixed crystal lattice via microwave-assisted hydrothermal method. *Mater Chem Phys* 2009, **116**: 269-272.

[54] Lee JH, Kim CK, Katoh S, *et al*. Microwave-hydrothermal versus conventional hydrothermal preparation of Ni- and Zn-ferrite powders. *J Alloy Compd* 2001, **325**: 276-280.

[55] Khollam YB, Deshpande SB, Khanna PK, *et al*. Microwave-accelerated hydrothermal synthesis of blue white phosphor: Sr_2CeO_4. *Mater Lett* 2004, **58**: 2521-2524.

[56] Zhang W, Lin D, Sun M, *et al*. Microwave hydrothermal synthesis and photocatalytic activity of $AgIn_5S_8$ for the degradation of dye. *J Solid State Chem* 2010, **183**: 2466-2474.

[57] Simoes AZ, Moura F, Onofre TB, *et al*. Microwave-hydrothermal synthesis of barium strontium titanate nanoparticles. *J Alloy Compd* 2010, **508**: 620-624.

[58] Chen X, Wang W, Chen X, *et al*. Microwave hydrothermal synthesis and upconversion properties of $NaYF_4$: Yb^{3+}, Tm^{3+} with microtube morphology. *Mater Lett* 2009, **63**: 1023-1026.

[59] Potdar HS, Deshpande SB, Deshpande AS, *et al*. Preparation of ceria-zirconia ($Ce_{0.75}Zr_{0.25}O_2$) powders by microwave-hydrothermal (MH) route. *Mater Chem Phys* 2002, **74**: 306-312.

[60] Ji H, Yang G, Miao X, *et al*. Efficient microwave hydrothermal synthesis of nanocrystalline orthorhombic $LiMnO_2$ cathodes for lithium batteries. *Electrochim Acta* 2010, **55**: 3392-3397.

[61] Vicente I, Cesteros PS, Guirado F, *et al*. Fast microwave synthesis of hectorite. *Appl Clay Sci* 2009, **43**: 103-107.

[62] Al-Tuwirqi RM, Al-Ghamdi AA, Al-Hazmi F, *et al*. Synthesis and physical properties of mixed Co_3O_4/CoO nanorods by microwave hydrothermal technique. *Superlattice Microst* 2011, **50**: 437-448.

[63] Yamauchi T, Tsukahara Y, Sakata T, *et al*. Barium ferrite powders prepared by microwave-induced hydrothermal reaction and magnetic property. *J Magn Magn Mater* 2009, **321**: 8-11.

[64] Cao SW, Zhu YJ, Cheng GF, *et al*. $ZnFe_2O_4$ nanoparticles: Microwave-hydrothermal ionic liquid synthesis and photocatalytic property over phenol. *J Hazard Mater* 2009, **171**: 431-435.

[65] Cao SW, Zhu YJ, Cui JB. Iron hydroxyl phosphate microspheres: Microwave-solvothermal ionic liquid synthesis, morphology control, and photoluminescent properties. *J Solid State Chem* 2010, **183**: 1704-1709.

[66] Cao SW, Zhu YJ. Iron oxide hollow spheres: Microwave-hydrothermal ionic liquid preparation, formation mechanism, crystal phase and morphology control and properties. *Acta Mater* 2009, **57**: 2154-2165.

[67] Yin S, Luo Z, Xia J, *et al*. Microwave-assisted synthesis of Fe_3O_4 nanorods and nanowires in an ionic liquid. *J Phys Chem Solids* 2010, **71**: 1785-1788.

[68] Dong WS, Li MY, Liu C, *et al*. Novel ionic liquid assisted synthesis of SnO_2 microspheres. *J Colloid Interf Sci* 2008, **319**: 115-122.

[69] Wang Y, Zhou A, Yang Z. Preparation of hollow TiO_2 microspheres by the reverse microemulsions. *Mater Lett* 2008, **62**: 1930-1932.

[70] Tang Z, Hu L, Zhang Z, *et al*. Hydrothermal synthesis of high surface area mesoporous lithium aluminate. *Mater Lett* 2007, **61**: 570-573.

[71] Liu S, Lebedev OI, Mertens M, *et al*. The merging of silica-surfactant microspheres under hydrothermal conditions. *Micropor Mesopor Mat* 2008, **116**: 141-146.

[72] Khan F, Eswaramoorthy M, Rao CN. Macroporous silver monoliths using a simple surfactant. *Solid State Sci* 2007, **9**: 27-31.

[73] Turta NA, De Luca P, Bilba N, *et al*. Synthesis of titanosilicate ETS-10 in presence of cetyltrimethylammonium bromide. *Micropor Mesopor Mat* 2008, **112**: 425-431.

[74] Wang S, Xiu H, Qian L, *et al*. CTAB-assisted synthesis and photocatalytic property of CuO hollow microspheres. *J Solid State Chem* 2009, **182**: 1088-1093.

[75] Zhao Z, Zhang L, Dai H, *et al*. Surfactant-assisted solvo- or hydrothermal fabrication and characterization of high-surface-area porous calcium carbonate with multiple morphologies. *Micropor Mesopor Mat* 2011, **138**: 191-199.

[76] Xu C, Zou D, Wang L, *et al*. γ-Bi_2MoO_6 nanoplates: Surfactant-assisted hydrothermal synthesis and optical properties. *Ceram Int* 2009, **35**: 2099-2102.

[77] Meng X, Zhang L, Dai H, *et al*. Surfactant-assisted hydrothermal fabrication and visible-light-driven photocatalytic degradation of methylene blue over multiple morphological $BiVO_4$ single-crystallites. *Mater Chem Phys* 2011, **125**: 59-65.

[78] García-Benjume ML, Espitia-Cabrera MI, Contreras-García ME. Hierarchical macro-mesoporous structures in the system TiO_2-Al_2O_3, obtained by hydrothermal synthesis using Tween-20® as a directing agent. *Mater Charact* 2009, **60**: 1482-1488.

[79] Zhao Q, Wang YG. A facile two-step hydrothermal route for the synthesis of low-dimensional structured Bi_2Te_3 nanocrystals with various morphologies. *J Alloy Compd* 2010, **497**: 57-61.

[80] Zhang A, Zhang J. Characterization of visible-light-driven $BiVO_4$ photocatalysts synthesized via a surfactant-assisted hydrothermal method. *Spectrochim Acta A* 2009, **73**: 336-341.

[81] Qu L, He C, Yang Y, *et al*. Hydrothermal synthesis of alumina nanotubes templated by anionic surfactant. *Mater Lett* 2005, **59**: 4034-4037.

[82] Wang Y, Zhang S, Wei K, *et al*. Hydrothermal synthesis of hydroxyapatite nanopowders using cationic surfactant as a template. *Mater Lett* 2006, **60**: 1484-1487.

[83] Jing Z, Han D, Wu S. Morphological evolution of hematite nanoparticles with and without surfactant by hydrothermal method. *Mater Lett* 2005, **59**: 804-807.

[84] Ji GB, Tang SL, Ren SK, *et al*. Simplified synthesis of single-crystalline magnetic $CoFe_2O_4$ nanorods by a surfactant-assisted hydrothermal process. *J Cryst Growth 2004*, **270**: 156-161.

[85] Wang J, Hojamberdiev M, Xu Y, *et al*. Nonionic surfactant-assisted hydrothermal synthesis of YVO_4: Eu^{3+} powders in a wide pH range and their luminescent properties. *Mater Chem Phys 2011*, **125**: 82-86.

[86] Sun G, Cao M, Wang Y, *et al*. Anionic surfactant-assisted hydrothermal synthesis of high-aspect-ratio ZnO nanowires and their photoluminescence property. *Mater Lett* 2006, **60**: 2777-2782.

[87] Wang YX, Sun J, Fan XY, *et al*. ACTAB-assisted hydrothermal and solvothermal synthesis of ZnO nanopowders. *Ceram Int* 2011, **37**: 3431-3436.

[88] Yan H, Zhang XH, Wu JM, *et al*. The use of CTAB to improve the crystallinity and dispersibility of ultrafine magnesium hydroxide by hydrothermal route. *Powder Technol* 2008, **188**: 128-132.

[89] Flaschen SS. An aqueous synthesis of barium titanate. *J Am Chem Soc* 1955, **77**: 6194-6194.

[90] McCormick MA, Slamovich EB. Microstructure development and dielectric properties of hydrothermal $BaTiO_3$ thin films. *J Eur Ceram Soc* 2003, **23**: 2143-2152.

[91] Lee B, Kim H, Cho S. Hydrothermal preparation of $BaTiO_3$ powders from modified hydroxide precursors. *Ferroelectrics* 2006, **333**: 233-241.

[92] Habib A, Haubner R, Stelzer N. Effect of temperature, time and particle size of Ti precursor on hydrothermal synthesis of barium titanate. *Mat Sci Eng B* 2008, **152**: 60-65.

[93] Hakuta Y, Ura H, Hayashi H, *et al*. Continuous production of $BaTiO_3$ nanoparticles by hydrothermal synthesis. *Ind Eng Chem Res* 2005, **44**: 840-846.

[94] Zhu X, Zhenghai Z, Zhu J, *et al*. Morphology and atomic-scale surface structure of barium titanate nanocrystals formed at hydrothermal conditions. *J Cryst Growth* 2009, **311**: 2437-2442.

[95] Oledzka M, Brese NE, Riman RE. Hydrothermal synthesis of $BaTiO_3$ on a titanium-loaded polymer support. *Chem Mater* 1999, **11**: 1931-1935.

[96] Chen C, Wei Y, Jiao X, *et al*. Hydrothermal synthesis of $BaTiO_3$: Crystal phase and the Ba^{2+} ions leaching behavior in aqueous medium. *Mater Chem Phys* 2008, **110**: 186-191.

[97] Cruz D, Bulbulian S, Lima E, *et al*. Kinetic analysis of the thermal stability of lithium silicates (Li_4SiO_4 and Li_2SiO_3). *J Solid State Chem* 2006, **179**: 909-916.

[98] Tang T, Zhang Z, Meng JB, *et al*. Synthesis and characterization of lithium silicate powders. *Fusion Eng Des* 2009, **84**: 2124-2130.

[99] Furusawa SI, Kamiyama A, Tsurui T. Fabrication and ionic conductivity of amorphous lithium meta-silicate thin film. *Solid State Ionics* 2008, **179**: 536-542.

[100] Furusawa SI, Kasahara T, Kamiyama A. Fabrication and ionic conductivity of Li_2SiO_3 thin film. *Solid State Ionics* 2009, **180**: 649-653.

[101] Naik YP, Mohapatra M, Dahale ND, *et al*.

Synthesis and luminescence investigation of RE^{3+} (Eu^{3+}, Tb^{3+} and Ce^{3+})-doped lithium silicate (Li_2SiO_3). *J Lumin* 2009, **129**: 1225-1229.

[102] Morimoto S, Khonthon S, Ohishi Y. Optical properties of Cr^{3+} ion in lithium metasilicate $Li_2O{\cdot}SiO_2$ transparent glass-ceramics. *J Non-Cryst Solids* 2008, **354**: 3343-3347.

[103] Zhang B, Nieuwouldt M, Easteal AJ. Sol–gel route to nanocrystalline lithium metasilicate particles. *J Am Ceram Soc* 2008, **91**: 1927-1932.

[104] Khomane RB, Sharma BK, Saha S, *et al*. Reverse microemulsion mediated sol–gel synthesis of lithium silicate nanoparticles under ambient conditions: Scope for CO_2 sequestration. *Chem Eng Sci* 2006, **61**: 3415-3418.

[105] Mondragón-Gutiérrez G, Cruz D, Pfeiffer H, *et al*. Low temperature synthesis of Li_2SiO_3: Effect on its morphological and textural properties. *Research Letters in Materials Science* 2008, **25**: 2513-2522 .

[106] Linkson PB, Phillips BD, Rowles CD. Computer methods for the generation of Eh-pH diagrams. *Minerals Sci Eng* 1979, **11**: 65-79.

[107] Dias A. Thermodynamic studies as predictive tools of the behavior of electroceramics under different hydrothermal environments. *J Solution Chem* 2009, **38**: 843-856.

[108] Lencka MM, Riman RE. Synthesis of lead titanate: Thermodynamic modeling and experimental verification. *J Am Ceram Soc* 1993, **76**: 2649-2659.

[109] Lencka MM, Riman RE. Thermodynamic modeling of hydrothermal synthesis of ceramic powders. *Chem Mater* 1993, **5**: 61-70.

[110] Lencka MM, Riman RE. Thermodynamics of the hydrothermal synthesis of calcium titanate with reference to other alkaline-earth titanates. *Chem Mater* 1995, **7**: 18-25.

[111] Information on www.factsage.com.

[112] Ortiz Landeros J, Contreras García ME, Gómez Yáñez C, *et al*. Surfactant-assisted hydrothermal crystallization of nanostructured lithium metasilicate (Li_2SiO_3) hollow spheres: Synthesis, structural and microstructural characterization. *J Solid State Chem* 2011, **184**: 1304-1311.

[113] Sing K. The use of nitrogen adsorption for the characterisation of porous materials. *Colloid Surface A* 2001, **187**: 3-9.

[114] Leofanti G, Padovan M, Tozzola G, *et al.* Surface area and pore texture of catalysts. *Catal Today* 1998, **41**: 207-219.

[115] Sing KS, Everett DH, Haul RA, *et al*. Reporting physisorption data for gas/solid systems with special reference to the determination of surface area and porosity. *Pure Appl Chem* 1985, **57**: 603-619.

[116] Ringgaard E, Wurlitzer T. Lead-free piezoceramics based on alkali niobates. *J Eur Ceram Soc* 2005, **25**: 2701-2706.

[117] Hao J, Wang X, Chen R, *et al*. Synthesis of $(Bi_{0.5}Na_{0.5})TiO_3$ nanocrystalline powders by stearic acid gel method. *Mater Chem Phys* 2005, **90**: 282-285.

[118] Fu ST, Hong LD, Wan C, *et al*. Preparation and properties of $(K_{0.5}Na_{0.5})NbO_3$-$LiNbO_3$ ceramics. *Trans Nonferrous Met Soc China* 2006, **16**: 466-469.

[119] Wang Y, Yi Z, Li Y, *et al*. Hydrothermal synthesis of potassium niobate powders. *Ceram Int* 2007, **33**: 1611-1615.

[120] Lu CH, Lo SY, Lin HC. Hydrothermal synthesis of nonlinear optical potassium niobate ceramic powder. *Mater Lett* 1998, **34**: 172-176.

[121] Jing X, Li Y, Yin Q. Hydrothermal synthesis of $Na_{0.5}Bi_{0.5}TiO_3$ fine powders. *Mater Sci Eng B* 2003, **99**: 506-510.

[122] Lin D, Xiao D, Zhu J, *et al*. Synthesis and piezoelectric properties of lead-free piezoelectric $[Bi_{0.5}(Na_{1-x-y}K_xLi_y)_{0.5}]TiO_3$ ceramics. *Mater Lett* 2004, **58**: 615-618.

[123] Peng C, Gong W. Preparation and properties of $(Bi_{1/2}Na_{1/2})TiO_3$-$Ba(Ti,Zr)O_3$ lead-free piezoelectric ceramics. *Mat Lett* 2005, **59**: 1576-1580.

[124] Wang X, Chan HL, Choy C. Piezoelectric and dielectric properties of CeO_2-added $(Bi_{0.5}Na_{0.5})_{0.94}Ba_{0.06}TiO_3$ lead-free ceramics. *Solid State Comm* 2003, **125**: 395-399.

[125] Jaeger RE, Egerton L. Hot pressing of potassium-sodium niobates. *J Am Ceram Soc* 1962, **45**: 209-213.

[126] Wu L, Zhang JL, Wang CL, *et al*. Influence of compositional ratio K/Na on physical properties in $(K_xNa_{1-x})NbO_3$ ceramics. *J Appl Phys* 2008, **103**: 084116.

[127] Shiratori Y, Magrez A, Pithan C. Particle size effect on the crystal structure symmetry of $K_{0.5}Na_{0.5}NbO_3$. *J Eur Ceram Soc* 2005, **25**: 2075-2079.

[128] Chowdhury A, Bould J, Zhang Y, *et al*. Nano-powders of $Na_{0.5}K_{0.5}NbO_3$ made by a sol-gel method. *J Nanopart Res* 2010, **12**: 209-215.

[129] Chowdhury A, O'Callaghan S, Skidmore TA, *et al*. Nanopowders of $Na_{0.5}K_{0.5}NbO_3$ prepared by the

Pechini method. *J Am Ceram Soc* 2009, **92**: 758-761.

[130] Sun C, Xing X, Chen J, *et al*. Hydrothermal synthesis of single krystalline (K, Na)NbO_3 powders. *Eur J Inorg Chem* 2007, **18**: 1884-1888.

[131] Lv JH, Zhang M, Guo M, *et al*. Hydrothermal synthesis and characterization of $K_xNa_{(1-x)}NbO_3$ powders. *Int J Appl Ceram Technol* 2007, **4**: 571-577.

[132] Santos IC, Loureiro LH, Silva MF, *et al*. Studies on the hydrothermal synthesis of niobium oxides. *Polyhedron* 2002, **21**: 2009-2015.

[133] Wang X, Zheng S, Zhang Y. A novel method to prepare ultrafine potassium tantalate powders. *Mater Lett* 2008, **62**: 1212-1214.

[134] Liu JF, Li XL, Li YD. Synthesis and characterization of nanocrystalline niobates. *J Cryst Growth* 2003, **247**: 419-424.

[135] Maeda T, Takiguchi N, Ishikawa M, *et al*. (K, Na)NbO_3 lead-free piezoelectric ceramics synthesized from hydrothermal powders. *Mater Lett* 2010, **64**: 125-128.